Communication

Creep Behavior at 1273 K (1000 °C) in Nb-Bearing Austenitic Heat-Resistant Cast Steels Developed for Exhaust Component Applications

YINHUI ZHANG, MEI LI, LARRY A. GODLEWSKI, JACOB W. ZINDEL, and QIANG FENG

A series of Nb-bearing austenitic heat-resistant cast steels with variations of N/C ratios were investigated, and the morphological change of Nb(C,N) from faceted blocks, mixed flake-blocks to "Chinese-script" was observed as N/C ratios decreased. The creep behavior of these alloys was studied at 1273 K (1000 °C), and the longest creep life and lowest creep rate occurred in model alloys with script Nb(C,N). Residual δ-ferrites and $(Cr,Fe)_{23}C_6$ were adverse to creep properties. This work indicates that the control of N/C ratio is required for the as-cast microstructural strengthening.

DOI: 10.1007/s11661-016-3544-1

To comply with more stringent environmental and fuel consumption regulations being standardized globally, exhaust gas temperatures from gasoline powertrains of automobiles are now reaching 1323 K (1050 °C), resulting in the skin temperature of exhaust components as high as 1273 K (1000 °C).[1] This leads to a significant temperature increase of about 200 K (200 °C) compared to the conventional standard.[2] Exhaust manifolds and turbine housings made of cast irons and ferritic steels are subjected to many failure events under such stricter conditions, including oxidation and creep cracks.[3] Thus, there is an urgent demand from automobile industries to develop novel and low-cost materials that are durable against these increased temperatures.

YINHUI ZHANG, Ph.D. Candidate, and QIANG FENG, Professor, are with the State Key Laboratory for Advanced Metals and Materials, University of Science and Technology Beijing, Beijing, 100083, China. Contact e-mail: qfeng@skl.ustb.edu.cn MEI LI, Technical Leader, LARRY A. GODLEWSKI, Research Engineer, and JACOB W. ZINDEL, Technical Specialist, are with the Ford Research and Advanced Engineering Laboratory, Ford Motor Company, Dearborn, MI 48124-4356.

Manuscript submitted October 1, 2015.
Article published online May 5, 2016

Nb-bearing austenitic stainless steels are potential candidates for developing novel alloys, owning to their improved oxidation resistance and mechanical properties.[4] These steels are extensively used in energy conversion systems, such as boiler/steam turbine power plants, and demonstrate promising creep resistance at temperatures near 1073 K (800 °C).[5] In the current research, substantial efforts have been dedicated to develop the cast grade of these steels, with improved creep resistance at 1273 K (1000 °C). Three crucial alloy design requirements are stabilizing the austenitic single-phase matrix, strengthening grain boundaries and interdendritic regions, and eliminating deleterious aging-induced phases (σ, Laves, *etc.*).[6–8] Economic factors should also be considered so that a 20Cr-10Ni type austenitic steel is selected, instead of a 25Cr-20/30Ni (HK/HP type) steel which is more prevalently used at high temperatures.[9] C and N, both of which are powerful austenite stabilizers and Nb(C,N)-forming elements, are introduced into the experimental alloys, with variations of N/C ratio. As a result, a high volume fraction of Nb(C,N) is expected to precipitate in the matrix of these novel alloys.

To date, in contrast to extensive studies on the strengthening effect of Nb(C,N) secondary precipitation during creep tests, relatively limited research has been conducted to investigate the strengthening effect of primary Nb(C,N), a common primary phase in cast steels.[4,10] Moreover, relevant investigations were mainly carried out at temperatures lower than 1273 K (1000 °C), due to previous lack of high-temperature industrial requirements.[6,11] Although primary Nb(C,N) may exhibit adverse effects on ductile fracture, its role in creep behavior and strengthening remains unclear, especially at temperatures above 1273 K (1000 °C).[12] The objective of the current research is to investigate the creep behavior in Nb-bearing austenitic heat-resistant cast steels developed for exhaust component applications. Of particular interest is to explore an applicable N/C ratio and as-cast microstructure for the improvement of creep resistance at 1273 K (1000 °C).

A series of Nb-bearing austenitic cast steels with variations of N/C ratio were designed and cast. The overall (C + N) content was maintained at a constant level (about 0.45 wt pct), except for alloy 2C4N with an increased overall content (0.59 wt pct). The experimental alloys were vacuum induction melted at China Iron & Steel Research Institute Group (CISRI) with high-purity raw metals (99.995 pct Fe, 99.98 pct Cr, 99.98 pct Ni, 99.999 pct Si, 99.5 pct Mn, 99.97 pct Nb, 99.999 pct C) and alloy CrN (83.3 pct Cr, 15.24 pct N, 0.05 pct Fe, 0.05 pct C, 0.003 pct Si, 0.03 pct P, 0.04 pct S, and 0.53 pct O). They were cast into cylindrical ingots with 80 mm in diameter and weighing ~20 kg each. The casting conditions were kept constant: pouring at 1823 K (1550 °C), followed by furnace cooling to 873 K (600 °C), then air cooling to room temperature.

The chemical compositions of the experimental alloys were quantitatively measured by NCS Testing Technology Co., Ltd. and are listed in Table I. Creep specimens were machined from the identical regions, about 5 mm away from each ingot surface with the specimen axis parallel to the ingot axis. These dog-bone specimens with a gage length of 25 mm and a cross-sectional diameter of 5 mm were used for creep rupture tests at 1273 K (1000 °C) and 50 MPa in air. The creep rupture tests for each experimental alloy have been carried out three times. Microstructural characterization was carried out using a ZEISS Axio Imager optical microscope (OM) and a ZEISS SUPRA 55 field emission-scanning electron microscope (FE-SEM) in secondary electron (SE) and backscattered electron (BSE) imaging modes. The average grain size was determined by using the standard linear intercept method. The area fraction of precipitates was assessed by calculating the area ratio of precipitates *via* the Image-Pro Plus software. The number density of primary Nb(C,N) at grain boundaries was estimated as the number of carbonitrides per unit length of grain boundaries.

The typical creep strain and creep strain rate curves of the experimental alloys as a function of time at 1273 K (1000 °C) and 50 MPa are plotted in Figures 1(a) and (b), respectively. Their average creep properties are summarized in Table II. The creep lives of these alloys are expressed in the descending order: alloys 4C0N, 3C2N, 2C4N, and 2C2N (Figure 1(a); Table II). Figure 1(b) suggests that alloys 3C2N and 4C0N exhibited an extended secondary or steady creep with significantly lower minimum creep rates. The secondary creep life in alloy 3C2N accounted for about 16 pct of its total creep life, whereas it increased to about 33 pct in alloy 4C0N. In contrast, the creep rate in alloys 2C2N and 2C4N dropped rapidly before a minimum value was established, and then the rate continuously increased until the specimen completely ruptured. Thus, the majority of creep life in these alloys was spent in the tertiary creep.

Figures 2(a) through (d) show the optical images showing the as-cast dendritic structure and the distribution of precipitates formed during casting. It is worth noting that the creep specimens of three alloys were composed of equiaxed grains, with the exception of alloy 3C2N. The average grain size of alloys 2C2N, 2C4N, and 4C0N was measured to be 984, 105, and 740 μm, respectively. For alloy 3C2N, the average width and length of columnar grains were determined to be 677 and 2539 μm, respectively, with the grain growth direction perpendicular to the load direction. Figure 2(a) illustrates the representative as-cast microstructure of alloy 2C4N, which was composed of austenitic matrix and a uniform dispersion of blocky and faceted precipitates within grains. The secondary dendritic segregation was not observed in this alloy. In contrast, alloys 2C2N, 3C2N, and 4C0N were composed of austenitic dendrites and duplex interdendrites, regardless of the eutectic morphology (Figures 2(b) through (d)). The average secondary dendrite arm spacing (SDAS) was measured to be 47.8, 49.1, and 51.8 μm, respectively. This confirmed the identical cooling rates during casting.

SEM-BSE images of the interdendritic regions and grain boundary areas are shown in Figure 3. The observed phases were identified by the combination of XRD and EPMA analyses. It is noted that the morphology of primary Nb(C,N) in alloy 2C4N exhibited blocky and faceted features, with occasionally lamellar growth extensions (Figure 3(a)). Figure 3(b) reveals that the interdendritic regions in alloy 2C2N consisted of flake-blocky Nb(C,N) and coarse vermicular δ-ferrites (gray contrast), whereas the interdendritic regions in both alloys 3C2N and 4C0N with relatively lower N/C ratios were dominant by typical "Chinese-script" Nb(C,N) (white contrast, Figures 3(c) and (d)). Therefore, based on the morphology of primary Nb(C,N), three alloy models were established: blocky (alloy 2C4N), flake-blocky (alloy 2C2N), and script (alloys 3C2N and 4C0N). A remarkable change in Nb(C,N) size was also observed, as well as the number density of Nb(C,N) that decorated grain boundaries. The number densities of Nb(C,N) at grain boundaries decreased in the order of alloys 4C0N (208/mm), 3C2N (112/mm), 2C4N (76/mm), and 2C2N (67/mm). It is interesting to note that the Nb(C,N) number density was proportional to the creep life of these alloys. Despite of these distinct differences in carbonitride morphology and number density, the area fraction of Nb(C,N) in the alloys was detected to be comparable (about 2.8 pct). The precipitation of cellular $(Cr,Fe)_{23}C_6$ and residual δ-ferrites was observed at grain boundaries in alloys 2C4N, 3C2N, and 4C0N, with the overall area fraction [$(Cr,Fe)_{23}C_6$ + δ] of 0.4, 1.4, and 1.1 pct, respectively (Figures 3(a), (c), and (d)). However, the area fraction of $(Cr,Fe)_{23}C_6$ and residual δ-ferrites in alloy 2C2N (3.1 pct) were significantly larger than those of the other alloys (Figure 3(b)).

In order to elucidate the failure mechanism that profoundly relates to the tertiary creep, microstructural evolution and creep crack propagation after creep rupture tests were examined from a longitudinal view (Figure 4). A majority of creep cracks was located near the fracture surface and was associated with the formation of δ-ferrites and $(Cr,Fe)_{23}C_6$. Figure 4(a) reveals that creep cracks in the blocky model alloy 2C4N propagated along grain boundaries. The precipitation and linkage of secondary $(Cr,Fe)_{23}C_6$ at grain

Table I. Measured Chemical Compositions of the Experimental Alloys (Weight Percent)

Alloy	Fe	Cr	Ni	Si	Mn	Nb	Ti	S	P	C	N	N + C	N/C
2C4N	bal.	21.32	9.88	0.92	0.95	2.18	0.013	0.007	0.014	0.23	0.36	0.59	1.57
2C2N	bal.	20.91	9.60	0.86	0.95	2.16	0.013	0.008	0.014	0.21	0.22	0.43	1.05
3C2N	bal.	19.68	10.12	0.80	0.93	2.09	0.005	0.008	0.013	0.29	0.15	0.44	0.52
4C0N	bal.	18.42	9.16	0.49	0.86	2.00	0.006	0.007	0.013	0.40	0.01	0.41	0

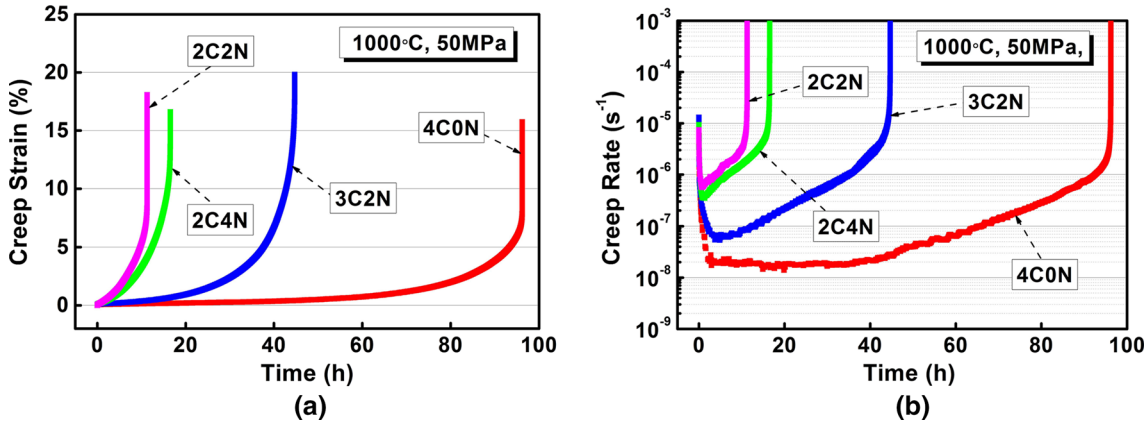

Fig. 1—Typical creep strain curve (*a*) and creep strain rate curve (*b*) of the experimental alloys as a function of time at 1273 K (1000 °C) and 50 MPa.

boundaries during creep tests seemed to accelerate the propagation of creep cracks. Figure 4(b) demonstrates that the interface between δ-ferrites and the austenitic matrix in alloy 2C2N was overwhelmingly vulnerable to crack. But unfortunately, these δ-ferrites formed during casting still remained stable even after creep exposure at 1273 K (1000 °C) for 15.3 hours. Figure 4(c) indicates that the creep cracks in alloy 4C0N preferentially nucleated and formed at $(Cr,Fe)_{23}C_6$ clusters, especially at those near grain boundaries. On the contrary, the primary "Chinese-script" Nb(C,N) appeared to retard the formation of creep cracks at both interdendritic regions and grain boundaries.

Creep rupture tests of the experimental alloys demonstrate that the creep property strongly depended on the as-cast microstructure. It suggests that longer creep lives and lower minimum creep rates occurred in script model alloys with relatively low N/C ratios. The current microstructural characterization reveals that the variation of N/C ratio gave rise to changes in the solidification path of the experimental alloys and subsequently altered the as-cast microstructure, including the morphology and distribution of primary Nb(C,N), the quantity of residual δ-ferrites and $(Cr,Fe)_{23}C_6$, and the macro-grain structure. Indeed, all of these metallurgical factors have affected the creep behavior of the experimental alloys at 1273 K (1000 °C) with the similar SDASs. Extensive studies have revealed that the formation of residual δ-ferrites at grain boundaries is adverse to oxidation and creep resistance at high temperatures,[6,13] while increasing the grain size with irregular, serrated grain boundaries will considerably improve the resistance to creep cracks.[14] Zhu *et al.* recognized that lamellar $(Cr,Fe)_{23}C_6$ at grain boundaries exhibited superior creep resistance than blocky $(Cr,Fe)_{23}C_6$ during creep tests at 1144 K (871 °C) in HK/HP steels.[15] Not only these lamellar $(Cr,Fe)_{23}C_6$ played an important role in preventing grain boundary sliding,[7,15] but they also showed detrimental thermal instability at this temperature.[15,16] In the current research, the formation of $(Cr,Fe)_{23}C_6$ was obviously inhibited by the formation of Nb(C,N), which was of much higher thermal stability at 1273 K (1000 °C). As the strengthening effect of $(Cr,Fe)_{23}C_6$ in HK40 steels, Nb(C,N) with different morphologies and distributions is also expected to be an important factor on the creep behavior of the experimental alloys.

Alloy 2C2N (flake–blocky model) manifested the worst creep resistance among all model alloys, in spite of the largest equiaxed grain size (Figure 1(a)). The early appearance of the tertiary creep after a small primary creep strain indicates that this alloy has not been effectively strengthened at 1273 K (1000 °C) (Figure 1(b)). Such property drop can be attributed to the effect of residual δ-ferrites, the amount of which was overwhelmingly larger than that of the other alloys. Residual δ-ferrites are inherently weaker than the austenitic matrix at temperatures higher than 1073 K (800 °C).[17] This resulted in creep cracks prone to nucleate and grow at the interface between δ-ferrites and the matrix, then propagate quickly until the specimen completely fractured (Figure 4(b)). Moreover, the lowest number density of primary Nb(C,N) at grain boundaries correspondingly decreased the strengthening ability at these areas. As a result, the creep rate increased rapidly after the minimum value was established. The deterioration of the creep property in alloy 2C2N implies the significance of stabilizing the austenitic matrix.

When the N/C ratio was increased to 1.57, the overall (C + N) content in alloy 2C4N (blocky model) suppressed the formation of residual δ-ferrites. However, comparing with alloy 2C2N, only a slight improvement of creep property was achieved in alloy 2C4N (Figure 1). The coarse blocky and faceted Nb(C,N) as well as the extremely fine equiaxed grain size are presumed to be the major limitations. The blocky Nb(C,N) are known to precipitate at temperatures even higher than the liquidus temperature of the alloy.[18,19] They acted as grain refiners, leading to the refined equiaxed grain size (Figure 2(a)). This refined grain size is adverse to creep properties and consequently accelerated the failure of this alloy. In addition, the coarse and blocky Nb(C,N) with a sparser distribution along grain boundaries could

Table II. Average Creep Properties of the Experimental Alloys Tested at 1273 K (1000 °C) and 50 MPa

Alloy	Creep Life (h)	Creep Strain (Pct)	Minimum Creep Rate ($\times 10^{-8}$ s^{-1})
2C4N	19.5 ± 2.2	16.9 ± 4.3	44.1 ± 8.0
2C2N	12.1 ± 1.3	15.3 ± 3.9	67.6 ± 6.5
3C2N	47.5 ± 9.6	19.9 ± 1.1	7.2 ± 1.9
4C0N	94.8 ± 13.0	15.4 ± 1.0	1.8 ± 0.6

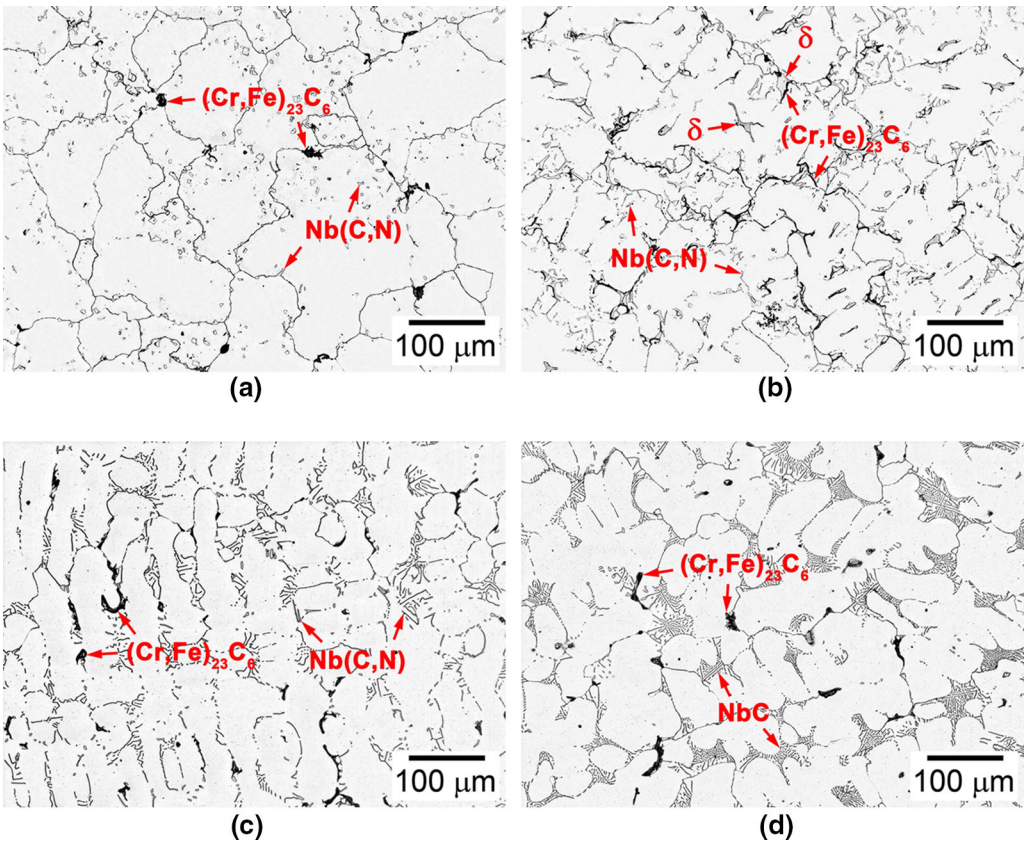

Fig. 2—Optical images of typical as-cast microstructures in alloys (*a*) 2C4N, (*b*) 2C2N, (*c*) 3C2N, and (*d*) 4C0N.

not prevent grain boundaries from sliding. The significant precipitation and linkage of secondary $(Cr,Fe)_{23}C_6$ at grain boundaries made the creep property even worse. Extensive studies on HK/HP steels have recognized that creep cracks would preferentially develop at the interface between $(Cr,Fe)_{23}C_6$ and the austenitic matrix.[16,20] As a result, these $(Cr,Fe)_{23}C_6$ weakened the grain boundaries through assisting the nucleation and propagation of creep cracks along grain boundaries (Figure 4(a)).

In comparison with alloys 2C2N and 2C4N, alloy 3C2N (script model) exhibited superior creep resistance, particularly the presence of the secondary creep (Figure 1(b)). This is predominantly ascribed to the development of the "Chinese-script" Nb(C,N) within the interdendritic regions. In general, interdendritic regions and grain boundaries are well recognized as the weakness for mechanical properties in cast alloys, since these last solidified regions usually contain remarkable concentration of casting segregations and defects.[21,22] The eutectic precipitation of primary "Chinese-script" Nb(C,N) with relatively small lamellar spacing strengthened these interdendritic regions. Moreover, the relatively higher number density of Nb(C,N) at serrated grain boundaries should make grain boundary sliding more difficult and also increased the path for grain boundary diffusion.[14] However, the columnar grains perpendicular to the load direction in alloy 3C2N were believed to hinder the further improvement of creep resistance. The increased transverse grain boundaries would facilitate the nucleation and coalescence of creep cracks, thereby accelerating the onset of the tertiary creep.

The longest creep life and the lowest creep rate occurred in alloy 4C0N, which is a script model alloy with the smallest N/C ratio (Figure 1). Compared to the primary Nb(C,N) in alloy 3C2N, the "Chinese-script" Nb(C,N) in alloy 4C0N was more refined, with decreased lamellar spacing of Nb(C,N) at the interdendritic regions and increased the number density of

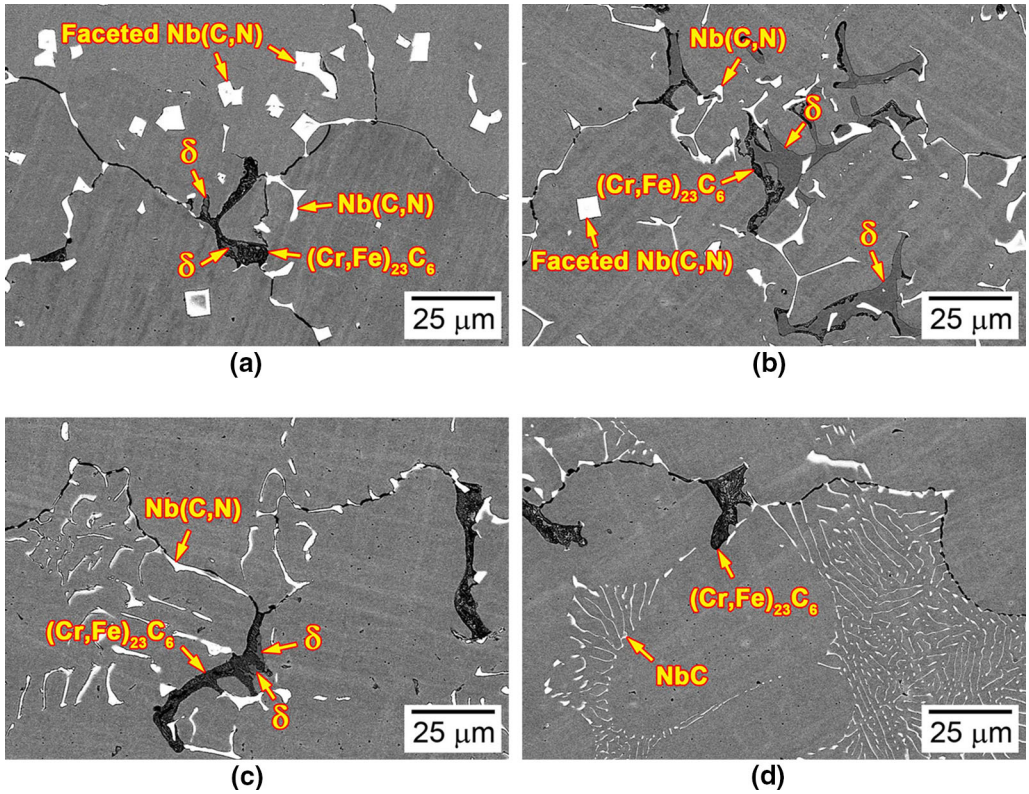

Fig. 3—SEM-BSE images of typical as-cast microstructures in alloys (*a*) 2C4N, (*b*) 2C2N, (*c*) 3C2N, and (*d*) 4C0N.

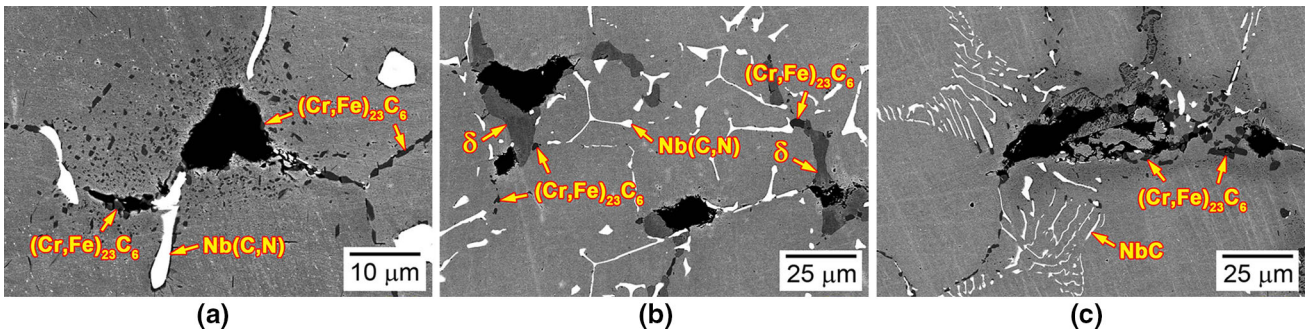

Fig. 4—SEM-BSE images of creep cracks close to the fracture surface in gage position after creep rupture tests at 1273 K (1000 °C) and 50 MPa in air: (*a*) alloy 2C4N, (*b*) alloy 2C2N, and (*c*) alloy 4C0N.

Nb(C,N) at grain boundaries (Figure 3(d)). Therefore, although the creep strengthening factors in alloy 4C0N were similar to those in alloy 3C2N, the strengthening ability was significantly improved. Furthermore, the relatively large equiaxed grain size reduced the grain boundary areas, thus beneficial to the creep property. As a result, an extended secondary creep and long creep life were obtained (Figure 1(b)). In addition, the amount of cellular $(Cr,Fe)_{23}C_6$ that acted as direct crack source during creep deformation (Figure 4(c)) should be decreased to further improve the creep property.

To summarize, the creep behavior at 1273 K (1000 °C) was investigated in a series of Nb-bearing austenitic heat-resistant cast steels with variations of N/C ratio. Under the identical casting conditions, a morphology change of Nb(C,N) from faceted blocks, mixed flake-blocks to "Chinese-script" occurred as N/C ratios decreased. The script model alloys with the largest Nb(C,N) number density exhibited the longest creep life and the lowest creep rate among all experimental alloys. The residual δ-ferrites and $(Cr,Fe)_{23}C_6$ that were also determined by N/C ratio were recognized to be significantly adverse to the creep property of these alloys at 1273 K (1000 °C), since they accelerated the nucleation and propagation of creep cracks. This work indicates that an optimum microstructural strengthening requires the control of N/C ratio to lower than 0.52. More work regarding the effect of N/C ratio on microstructures and

mechanical properties using the computational thermodynamic calculations will be published elsewhere.

The authors would like to acknowledge W. W. Zheng, W. Y. Yang, and Y. R. Zheng for the assistance of creep rupture tests and the useful discussions. The financial support provided by Ford Motor Company (University Research Program) is also acknowledged.

REFERENCES

1. K. Matsumoto, M. Tojo, Y. Jinnai, N. Hayashi, and S. Ibaraki: *Mitsubishi Heavy Ind. Tech. Rev*., 2008, vol. 45, pp. 1–5.
2. N. Fukai, T. Imamura, K. Ito, and Y. Kuribayashi: *Hitachi Rev*., 2008, vol. 57, pp. 248–52.
3. M. Ike, K. Akiyama, K. Ohtsuka, and K. Itoh: *Int. J. Mater. Prod. Technol*., 1991, vol. 6, pp. 243–56.
4. J. Erneman, M. Schwind, H.O. Andrén, J.O. Nilsson, A. Wilson, and J. Ågren: *Acta Mater*., 2006, vol. 54, pp. 67–76.
5. Y. Yamamoto, M.P. Brady, Z.P. Lu, P.J. Maziasz, C.T. Liu, B.A. Pint, K.L. More, H.M. Meyer, and E.A. Payzant: *Science*, 2007, vol. 316, pp. 433–36.
6. J.P. Shingledecker, P.J. Maziasz, N.D. Evans, and M.J. Pollard: *Int. J. Pres. Ves. Pip*., 2007, vol. 84, pp. 21–28.
7. J.S. Zhang, P.E. Li, and J.Z. Jin: *Acta Metall*., 1991, vol. 39, pp. 3063–70.
8. S.J. Zhu, J. Zhao, and F.G. Wang: *Scripta Metall*., 1990, vol. 24, pp. 559–64.
9. K. Buchanan and M. Kral: *Metall. Mater. Trans. A*, 2012, vol. 43A, pp. 1760–69.
10. N.D. Evans, P.J. Maziasz, J.P. Shingledecker, and M.J. Pollard: *Metall. Mater. Trans. A*, 2010, vol. 41A, pp. 3032–41.
11. Y. Yamamoto, M.P. Brady, M.L. Santella, H. Bei, P.J. Maziasz, and B.A. Pint: *Metall. Mater. Trans. A*, 2011, vol. 42A, pp. 922–31.
12. J.H. Yoon, E.P. Yoon, and B.S. Lee: *Scripta Mater*., 2007, vol. 57, pp. 25–28.
13. Y. Yamamoto, M.L. Santella, M.P. Brady, H. Bei, and P.J. Maziasz: *Metall. Mater. Trans. A*, 2009, vol. 40A, pp. 1868–80.
14. J.M. Larson and S. Floreen: *Metall. Trans. A*, 1977, vol. 8A, pp. 51–55.
15. S.J. Zhu, J. Zhao, and F.G. Wang: *Metall. Trans. A*, 1990, vol. 21A, pp. 2237–41.
16. R. Voicu, J. Lacaze, E. Andrieu, D. Poquillon, and J. Furtado: *Mater. Sci. Eng. A*, 2009, vols. 510–511, pp. 185–89.
17. Y. Yamamoto, M.P. Brady, Z.P. Lu, C.T. Liu, M. Takeyama, P.J. Maziasz, and B.A. Pint: *Metall. Mater. Trans. A*, 2007, vol. 38A, pp. 2737–46.
18. E.R. Cutler, A.J. Wasson, and G.E. Fuchs: *Scripta Mater*., 2008, vol. 58, pp. 146–49.
19. Y.H. Zhang, M. Li, L.A. Godlewski, J.W. Zindel, and Q. Feng: *Acta Metall. Sin*., 2016, vol. 52, pp. 661–71.
20. M. Whittaker, B. Wilshire, and J. Brear: *Mater. Sci. Eng. A*, 2013, vol. 580, pp. 391–96.
21. E.R. Cutler, A.J. Wasson, and G.E. Fuchs: *J. Cryst. Growth*, 2009, vol. 311, pp. 3753–60.
22. B. Piekarski: *Mater. Charact*., 2010, vol. 61, pp. 899–906.